Stannern

Monomict Brecciated Eucrite, 52kg

Seen to fall

Figure 1: *Pieces of the Stannern eucrite. Both photos taken by Matteo Chinellato - National History Museum, Milano.*

Introduction: The Stannern eucrite (**Figure 1**) fell at 6:00 AM near Iglau, Jihomoravsky Region, Moravia, Czech Republic, on May 22nd, 1808 (von Schreibers, 1808). Though 200-300 stones fell in total, about 66 were recovered totaling 52 kilograms, the largest piece of which weighed approximately 7.6 kg; a

histogram showing the number and size of all recovered pieces and a map of their locations can be found in **Figure 2**, from Engelhardt (1963), after von Schreibers (1820). The largest remaining amount (14 kg) is currently housed at the Natural History Museum in Vienna, and other significant fractions of the original meteorite are housed at the University of Tübingen (4 kg), the National Museum in Budapest (2 kg), the Museum für Naturkunde in Berlin (1.1 kg), and the National Museum in Prague (1.2 kg) (Grady, 2000). An interactive photograph of Stannern, courtesy of the Natural History Museum of London, can be found at http://www.nhm.ac.uk/nature-online/virtual-wonders/vrmeteorite2.html.

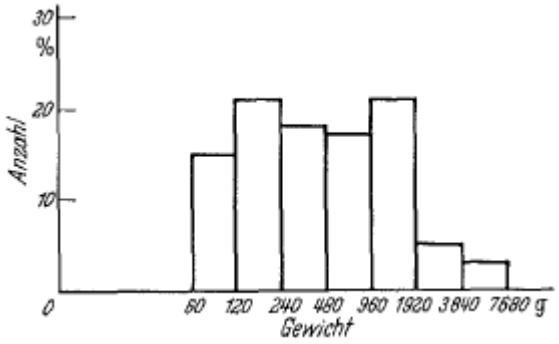

Gewicht in g	Zahl	%
60—120	10	15
120—240	14	21
240—480	12	18
480—960	11	17
960—1920	14	21
1920—3840	3	5
3840—7680	2	3
	66	

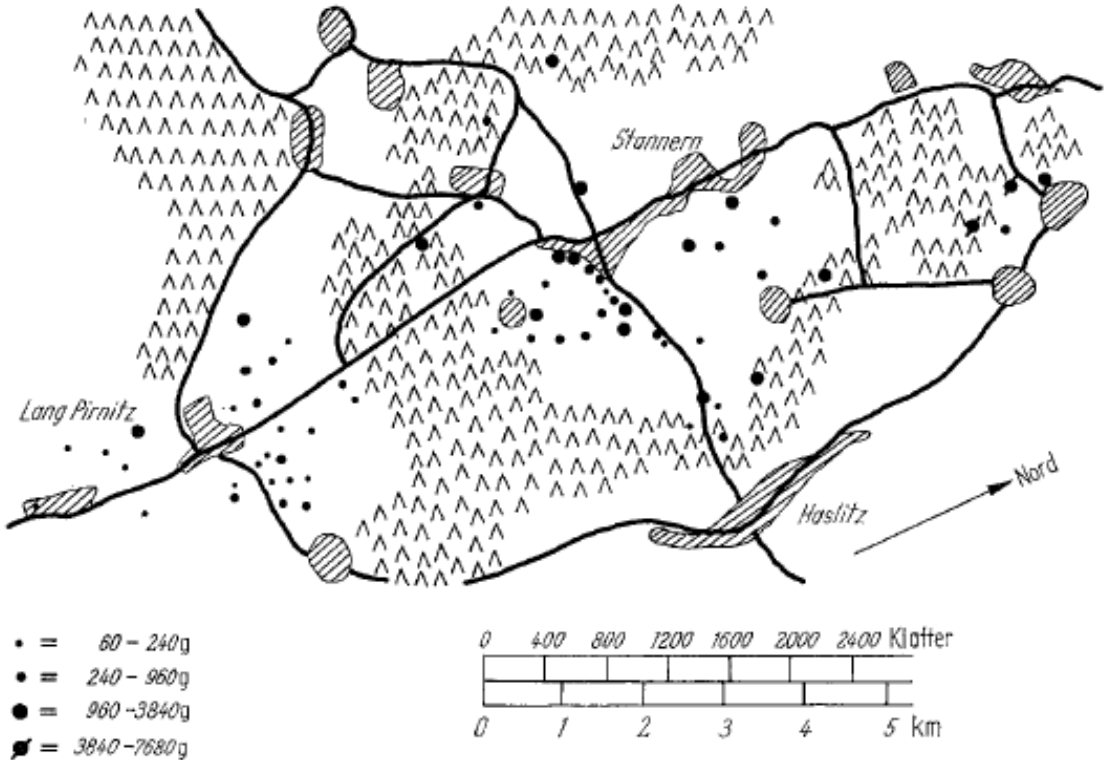

Figure 2*: Histogram , table, and map from Engelhardt (1963), after von Schreibers (1820), detailing the size and spatial distribution of pieces of the Stannern eucrite. Figures 1 and 2, Table 1 in Engelhardt (1963).*

Stannern is encased in a fusion crust with distinct zones. Engelhardt (1963) classified three different strata: an inner transition layer, a “middle” zone, and the outer crust (**Figure 3**). Zbik et al (1990) and Zbik and Gostin (1996a) described only two strata: the first is an outer homogenous, bubbly, well-

preserved, and well-mixed quenched glass, approximately ~200 µm thick, while the second 100-150 µm section has a denser, heterogeneous, more massive texture without bubbles, suggesting rapid and incomplete melting.

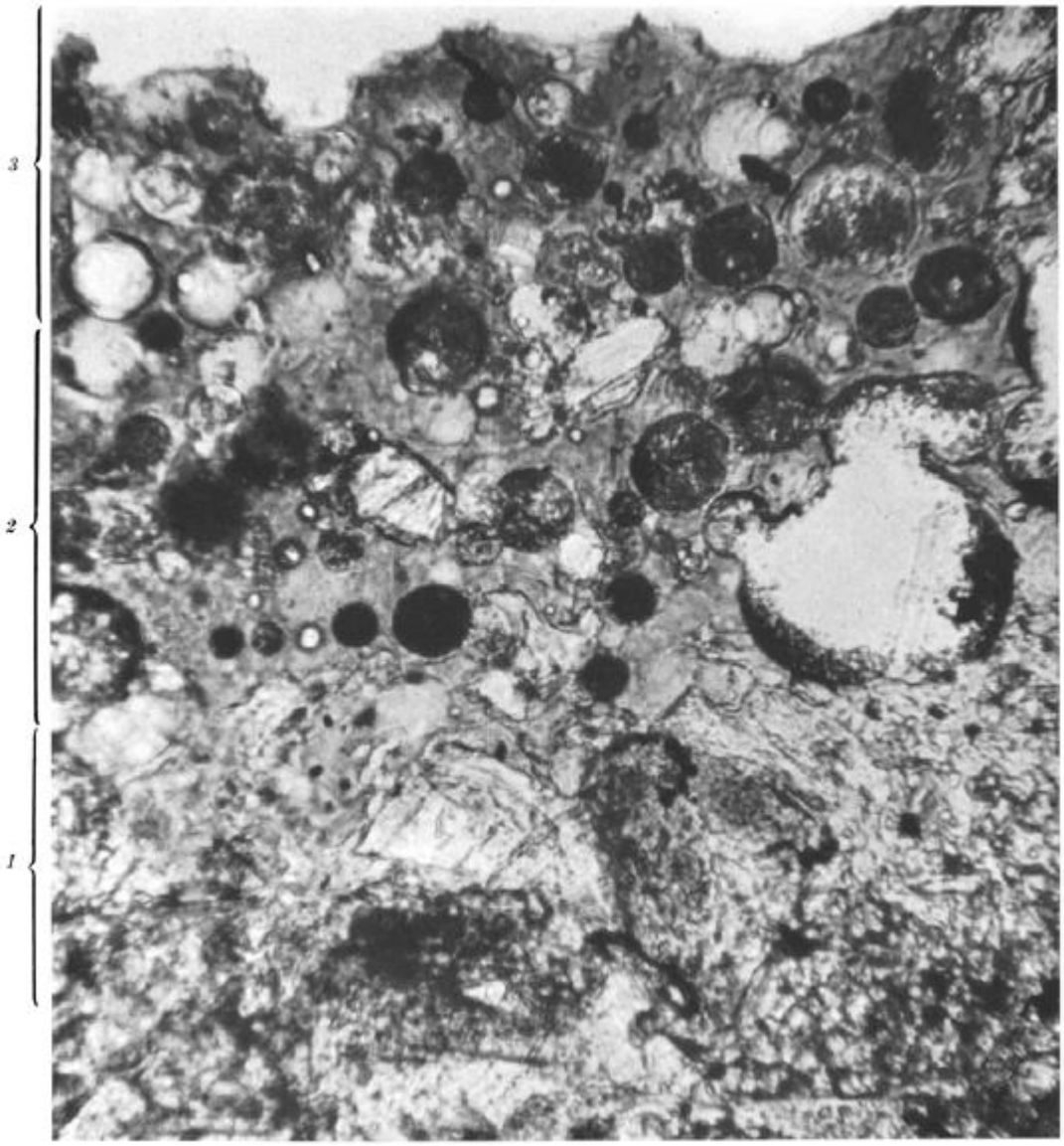

Figure 3*: Cross-section through the Stannern fusion crust, from Engelhardt (1963). 1 = Transition Zone ("Übergangszone"), 2 = Middle Zone ("Mittelzone"), 3 = Outer Zone ("Außenzone"). Width of field, from top to bottom, is 500 µm.*

Stannern is a monomict brecciated eucrite, with a complex crystallization, metamorphic (thermal and shock), and brecciation history. Its basic composition and mineralogy are similar to terrestrial basalts (although with much higher FeO), showing mostly coarse-grained basaltic clasts composed nearly entirely of pyroxene and plagioclase, set in a finer-grained matrix of similar materials.

Petrography: Stannern was analyzed by numerous researchers in the 19th and early 20th century (e.g. von Schreibers, 1808; von Schreibers, 1820; Rose, 1825; Rammelsberg, 1851; von Haidinger, 1862; Tschermak, 1872; Wahl, 1907; Michel, 1912; Merrill, 1916; Merrill, 1925; LaCroix, 1925) but was most

thoroughly described, analyzed, and summarized by Engelhardt (1963), who included an extensive survey and bibliography of previous research.

Stannern is composed nearly entirely of pyroxene (orthopyroxene and both high and low-Ca clinopyroxene) surrounding euhedral, lath-like anorthitic plagioclase, with variolitic, sub-ophitic, granulitic, gabbroic-ophitic (Metzler et al, 1995), and fasciculate (Walker et al, 1978a) clasts of up to 5mm-sized crystals (Kunz et al, 1995) set in a fine-grained, recystallized, comminuted glassy matrix of similar but variable-sized mineralogy (see **Table 1** for modal mineralogy, and **Figure 4** for a photo of an ophitic clast). The boundary between clasts and matrix, however, is gradational (Engelhardt, 1963).The

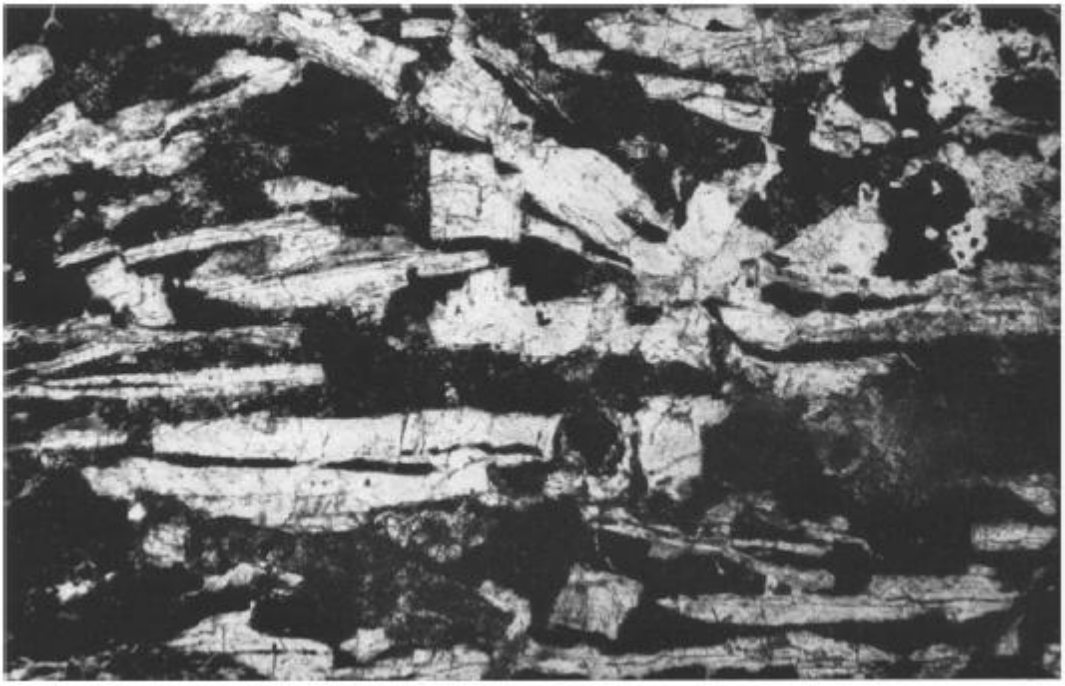

Figure 4*: Sub-ophitic to ophitic texture in Stannern clast; the lighter lath-like mineral is plagioclase surrounded by dark pyroxenes. Field of view is 2.1 mm x 3.3 mm. Figure 3 in Engelhardt (1963).*

larger clasts are up to 10 x 7 mm in size (Takeda and Graham, 1991). Other accessory minerals include ilmenite, troilite, chromite, quartz, zircon, and metal. Both plagioclase and pyroxene are “cloudy” in appearance due to numerous small inclusions of other minerals (e.g., chromite and ilmenite); these inclusions may represent the effect of extensive subsolidus heating and thermal autometamorphism (Harlow and Klimentidis, 1980), thermal annealing (Takeda et al, 1983), or slow subsolidus cooling after pyroxene exsolution had already taken place (Brearley et al, 1993), though the formation process for the inclusions may have been coupled with pyroxene exsolution (Metzler et al, 1995). The inclusion density may also be related to the degree of homogenization of the minerals (Takeda et al, 1983).

Engelhardt (1963) documented a distinct sequence of crystallization: euhedral plagioclase appeared first, followed by grey-brown hypersthene (showing 90^{o} cleavage planes) nucleated in the interstices between plagioclase laths, growing in sub-parallel alignment with plagioclase. Pigeonite formed next, both as distinct anhedral crystals and as irregular masses rimming hypersthene, taking on the same orientation as their hypersthene cores (and in some cases, totally enveloping hypersthene to form

Figure 5*: Hypersthene crystal (left, cloudy, with few obvious lamellae) rimmed by later pigeonite (right, translucent, with numerous lamellae); note that the transition is gradational in some places but sharp in others. The light-gray grain in the lower right corner is plagioclase. Field of view is 450 µm x 570 µm. Figure 7, Engelhardt (1963).*

pseudomorphs) (**Figure 5**). The latest pigeonites, augites, and last open voids in ophitic clasts contain inclusions of opaques (ilmenite, chromite, and troilite) and finally quartz, which nucleated last.

Takeda and Graham (1991) noted that the textures observed in Stannern are clearly polymict (i.e., sampling different textural lithologies), but the mineral chemistry across the sample is similar enough to be considered monomict. Other researchers (e.g. Metzler et al, 1995) have also invoked the variety of different clasts, including small granulite fragments, in describing Stannern as texturally polymict but chemically monomict.

Duke and Silver (1967) described the presence of dark brown opaque cryptocrystalline or glassy material in veins that have sharp boundaries with both clasts and the matrix, suggesting that the veins were formed after the accumulation of the breccia. The presence of these pseudotachylitic veins was also mentioned in Bobe (1992) and Metzler et al (1995), both of whom noted that they contain fragments of the adjacent host rock, and have a chemical composition similar to the bulk chemical composition of Stannern. Metzler et al (1995) also cites the presence of "intrusive melt dikes with quench textures," grouped separately from the pseudotachylites, that intersect both lithic clasts and the matrix; the texture of these dikes is dominated by chemically zoned pyroxenes in fine-grained matrix of pyroxene and feldspar laths.

	Silver and Maynes (1962) norm	Engelhardt (1963) mode	Duke and Silver (1967) mode	Duke and Silver (1967) norm	Delaney et al (1984e) mode
Pyroxene	54.39	54 (11% opx)	55	56.6	47.6
Plagioclase	35.74	36	39	35.9	42.8
Quartz	6.98	7	3	3.7	7.7
Other	2.89	3	3	3.8	1.9

Table 1: Basic Mineralogy of Stannern.

Mineral Chemistry:

Pyroxene: The bulk composition of pyroxenes in Stannern is pigeonitic (Engelhardt, 1963), though the composition of specific crystals varies from high-Fe/Mg orthopyroxene (hypersthene), to high-Fe/low-Ca clinopyroxene (pigeonite – $Fe_{62.2}Mg_{36.4}Ca_{1.4}$), to high-Ca clinopyroxene (augite – $Fe_{29}Mg_{31}Ca_{40}$) (Takeda et al, 1983), and there is some inversion of pigeonite to high-Fe (60%) orthopyroxene as well (Duke and Silver, 1967) (**Figure 6**). In addition to rare pigeonite exsolution lamellae in hypersthene (Engelhardt, 1963), there are numerous augite exsolution lamellae along (001) pigeonite planes, with extremely variable widths ranging from 70 nm to 3 μm (Brearley et al, 1993; Takeda et al, 1983); these augite lamellae are more abundant near the rims, but are of greater width (1-3 μm) and spaced further apart (20-30 μm) in the cores (Takeda et al, 1983) (**Figure 7**).

Most relict Fe/Mg zoning has been homogenized, though there is still some evidence of its original presence in Stannern pyroxenes (Takeda and Graham, 1991). However, remnant calcic zoning has been well-preserved in pigeonites, with average compositions at the cores ($Fe_{61.8}Mg_{36.5}Ca_{1.7}$) exhibiting much lower Ca contents than average compositions in the outermost 150 μm of a crystal ($Fe_{43}Mg_{31}Ca_{26}$) (Takeda et al, 1983) (**Figure 6**). Core to rim traverses (**Figure 8**) also show steady increases in calcium content (Takeda et al, 1983), though this analysis is complicated by the dominant presence of lamellae (in both cores and rims) with different chemical compositions. Takeda et al (1983) suggest two possibilities for chemical zoning in pyroxenes: first, Stannern pyroxenes were originally zoned (as mentioned in Duke and Silver, 1967) but homogenized by a later thermal event, or second, that Stannern pyroxenes crystallized with no zoning of Fe or Mg but with strong Ca zoning (but no mechanism is suggested by the authors for this case). Chemical zoning must also be interpreted in the framework of sequential crystallization cited by Engelhardt (1963), where Fe- and Mg-rich hypersthenes

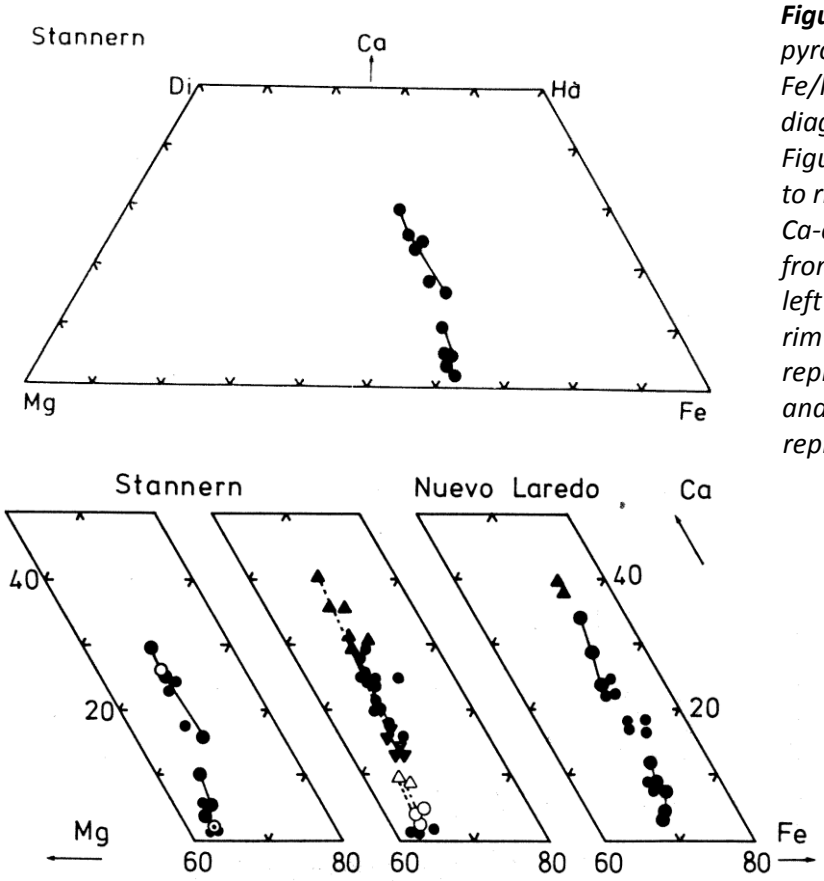

***Figure 6**: Variations in Stannern pyroxene chemistry, from high Fe/low Ca to low Fe/high Ca. Top diagram is from Takeda et al (1983), Figure 7, where lines represent core to rim traverses (moving towards Ca-enrichment). Bottom graphs are from the same source, Figure 11: left diagram shows similar core to rim traverses, where the open circle represents the bulk rim composition and the open circle with a dot represents the bulk core composition; right diagram shows host-lamallae exsolution pairs connected by tie lines, where rim compositions are represented by solid triangles, core compositions by open triangles and open circles, and other individual analyses by filled circles.*

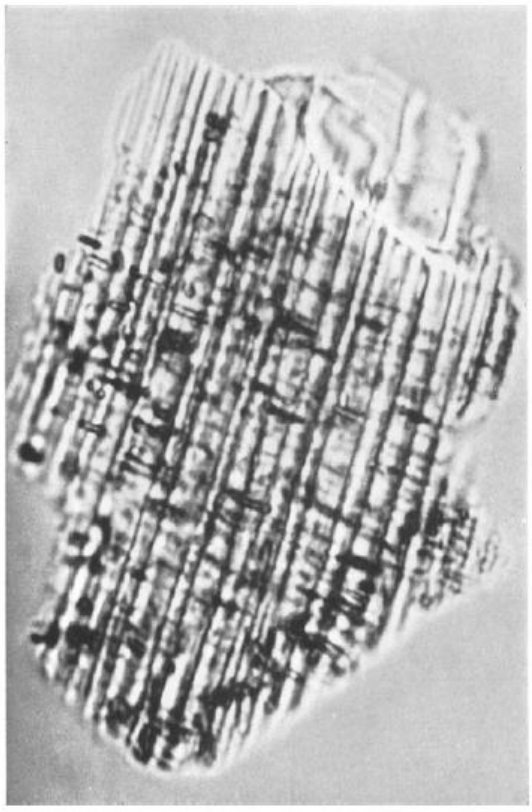

***Figure 7**: Isolated pigeonite grain (100 µm in length) showing clear augite exsolution lamellae along (001) planes. These lamellae are not twins because the planes are less refractive than the pigeonite surrounding them. Engelhardt (1963), Figure 8.*

cores are rimmed and in some cases completely replaced by later Ca-rich pigeonite and augite (though these minerals also formed separate grains) (**Figure 5**).

Most pyroxenes (especially orthopyroxene, see **Figure 5**) appear cloudy due to micron-submicron scale inclusions of ilmenite and chromite, with minor plagioclase, metallic iron, troilite, silica, and augite; while chromite was proposed by some researchers to be the main included phase (Duke and Silver, 1967; Boctor et al, 1987), other

investigations showed that the most numerous inclusions in Stannern pyroxenes are ilmenite (Engelhardt, 1963),

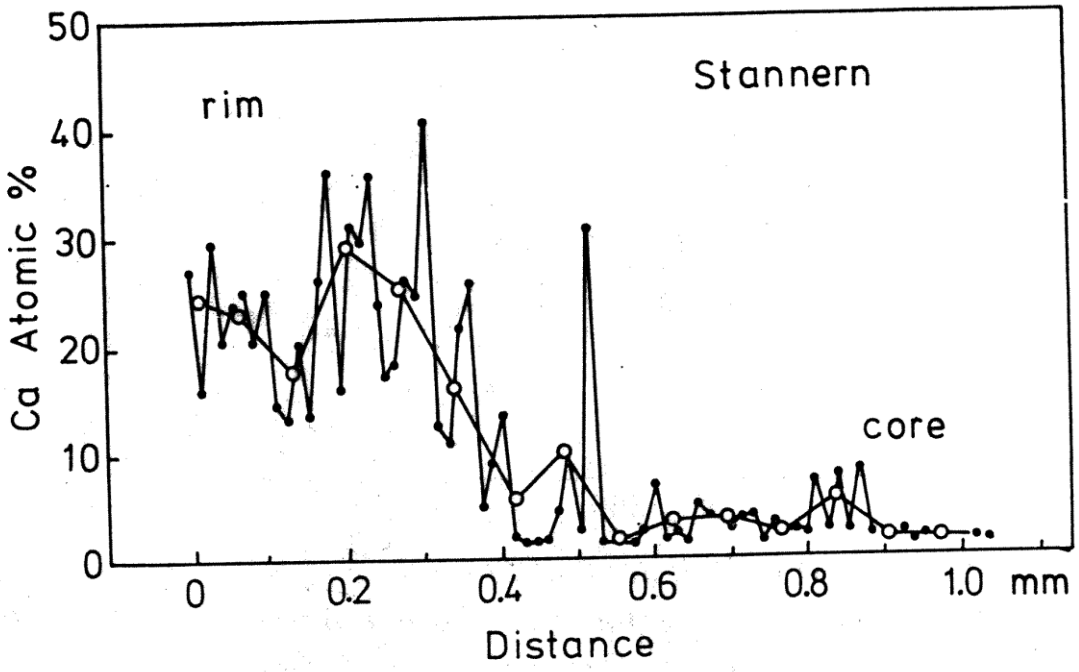

***Figure 8**: Core to rim traverse of pyroxene for Stannern; dark circles are point analyses from every 14 µm and open circles are the average trend for every 120 µm. Figure 12 from Takeda et al (1983).*

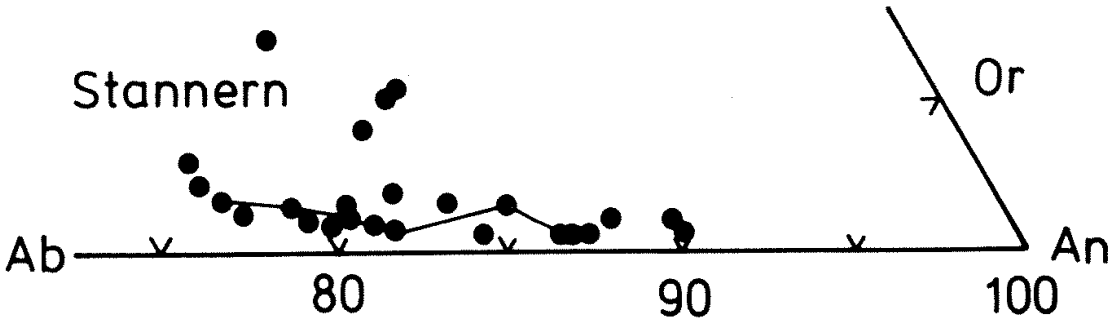

***Figure 9**: Plagioclase composition data from Stannern; lines represent core to rim traverses, from Na-rich to Ca-rich regions of the crystals. Some K-rich spots are present. From Figure 13, Takeda et al (1983).*

which may be due to high bulk TiO_2 content (Harlow and Klimentidis, 1980). These inclusions can be of different shapes (blebs, lenses, or prisms) in various textural settings (curved surfaces, twin boundaries, and exsolution intergrowth boundaries) and are usually oriented to some degree (Engelhardt, 1963; Harlow and Klimentidis, 1980).

Stannern pyroxenes are enriched in REEs relative to the main-group eucrite pyroxenes, with a pronounced negative Eu anomaly (Hsu and Crozaz, 1996).

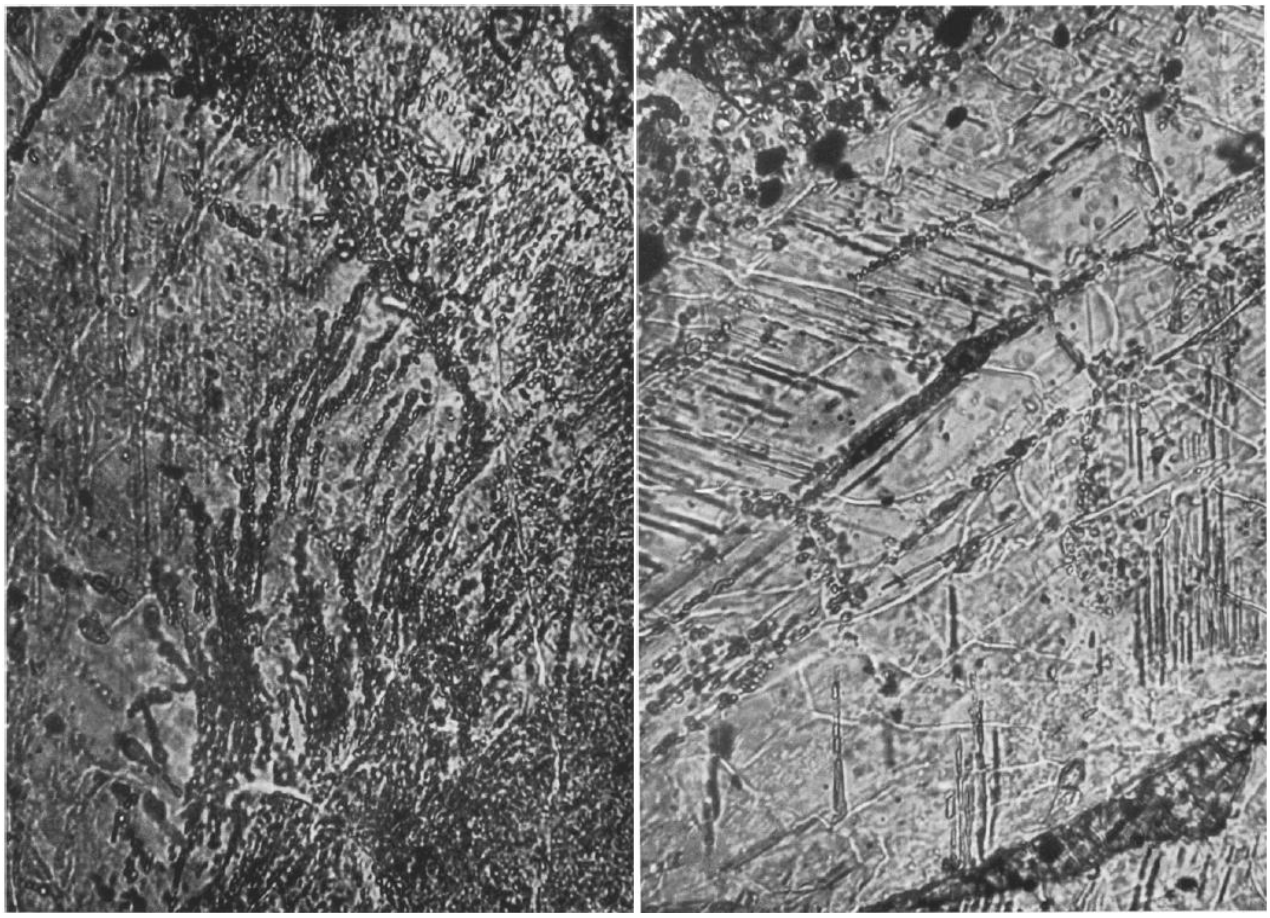

Figure 10*: Micron-scale droplet-shaped (left) and needle-shaped (right) inclusions of pyroxene in plagioclase. Note the apparent alignment of some, but not all inclusions. Field of view for both photos is 250 µm x 180 µm. Engelhardt (1963), figures 4 and 5.*

Plagioclase: Plagioclase composition in Stannern is variable but centered around 80% anorthitic, i.e., bytownite (Engelhardt, 1963; Duke and Silver, 1967; Boctor et al, 1987; Tera et al, 1987a) (**Figure 9**), but different types of twins within crystals have somewhat variable composition (Engelhardt, 1963). Some plagioclase crystals occur as laths with thin cores of pigeonite or blocky pyroxene (Fig. 10a in Takeda et al, 1983). Plagioclase is zoned, from Ca-rich cores to Na-rich rims, but this trend is not smooth, and there are unusual K-rich spots (Takeda et al, 1983) (**Figure 9**). These K-enriched areas may be related to shock or short-lived heating events (Delaney et al, 1984e). There is also a high concentration of sodium and barium in Stannern plagioclase compared to other eucrites, consistent with the bulk chemical composition of the meteorite (Takeda et al, 1983; Hsu and Crozaz, 1996). Metzler et al (1995) also observed a second generation of <20 µm feldspar grains in the matrix that are much more Ca-rich than the primary feldspar in the lithic clasts (An_{96} vs An_{81}).

Plagioclase crystals also contain micron-scale droplet and needle-shaped inclusions of other minerals (some of which are aligned) (**Figure 10**), causing a “cloudy” appearance; included minerals in plagioclase are texturally and chemically similar to those found in pyroxene (mainly Ca-rich pyroxene, i.e., pigeonite, with minor ilmenite and chromite) (Engelhardt, 1963; Harlow and Klimentidis, 1980).

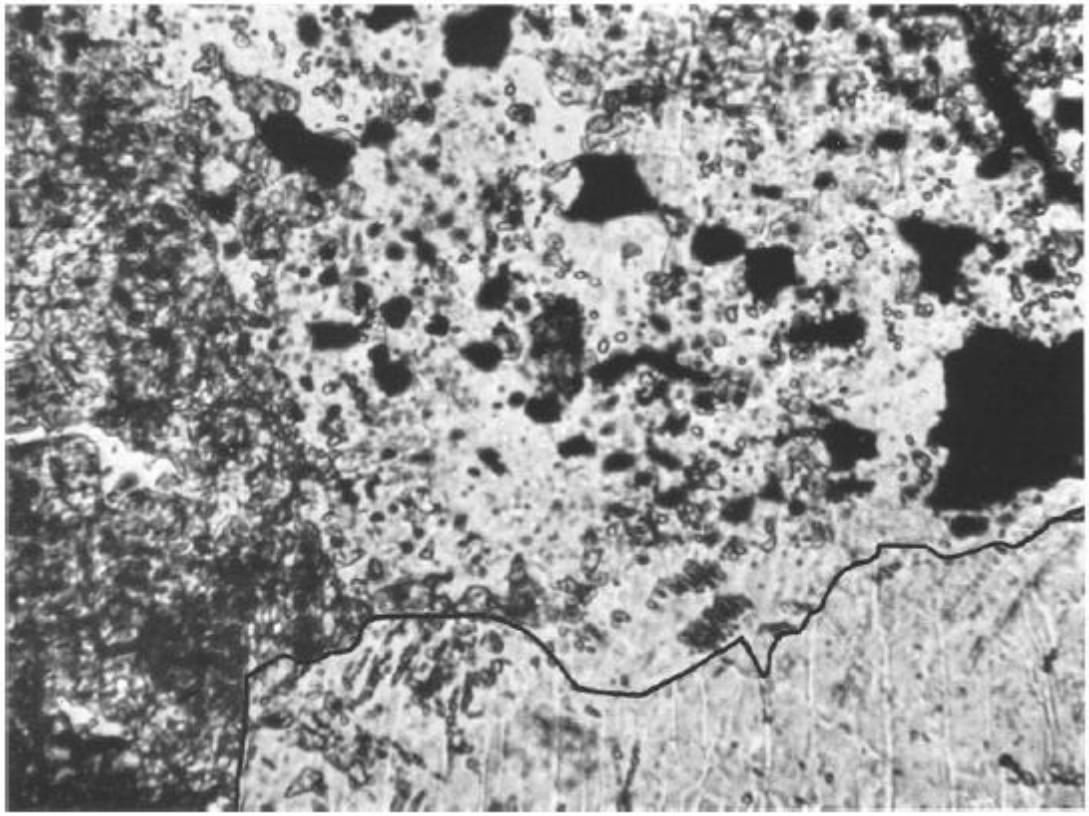

Figure 11*: Translucent quartz with inclusions of opaque minerals (troilite and ilmenite), as well as clear, refractive pyroxene droplets; the grain is bounded by dark gray pigeonite to the left and twinned plagioclase at the bottom. Field of view is 400 µm x 530 µm. Engelhardt (1963), Figure 9.*

Stannern plagioclase shows an enrichment for LREEs relative to chondrites, with a pronounced positive Eu anomaly, but reliable data on HREEs in plagioclase is elusive due to large numbers of pyroxene inclusions and low overall HREE abundances (Hsu and Crozaz, 1996).

Mesostasis: There is no evidence of preserved mesostasis glass in Stannern, but there are hints that a mesostatic phase was present and later metamorphosed, including fine, dusty, mottled areas at the junctions of pyroxene and plagioclase that have been recrystallized to aggregates of ilmenite and chromite, in addition to troilite, quartz, augite, and apatite (Takeda et al, 1983).

Ilmenite: Ilmenite in Stannern occurs in conjunction with quartz and troilite as intergrowths in both clastic and matrix portions of the meteorite (Engelhardt, 1963), as inclusions in pyroxene crystals and plagioclase rims (Engelhardt, 1963; Harlow and Klimentidis, 1980), in metamorphosed mesostatic glass (Takeda et al, 1983) and irregular grains in the matrix (Engelhardt, 1963; Bunch and Keil, 1971), which can be up to several hundred microns across (Ireland and Bukovanska, 1992). It also coexists with chromite occurrences (Bunch and Keil, 1971). Harlow and Klimentidis (1980) determined an Mg# of 3 for an included ilmenite and 2 for a “free” grain. Twinning was noted in Stannern ilmenites by Engelhardt (1963).

Chromite: Chromite occurs as an exsolved phase in pyroxenes, within augite lamellae and coherently along pigeonite-augite interfaces (Brearley et al, 1993). It also occurs as an accessory mineral along with quartz and troilite in metamorphosed mesostasis (Takeda et al, 1983).

Troilite: Troilite forms similarly to ilmenite, but also as larger elongated lenticular masses up to 1 cm in size. Duke and Silver (1967), Figure 8, shows a pyroxene grain being replaced by quartz and troilite; the authors suggest that this may be a response to late magmatic buildup of sulfur-rich vapors. Troilite also occurs as an accessory mineral in metamorphosed mesostasis glass (Takeda et al, 1983).

Quartz: Quartz was first identified in Stannern by Berwerth (1912). Engelhardt (1963) noted prominent masses in all of his Stannern thin sections, mostly associated with opaques in the last anhedral voids of the ophitic portions of the meteorite (**Figure 11**), and as inclusions in the latest-nucleated pigeonites. Some masses of quartz appear to have grown into embayed regions of plagioclase and pyroxene crystals. Quartz also occurs in metamorphosed mesostatic regions of the meteorite (Takeda et al, 1983).

Tridymite: Birck and Allegre (1978) report finding tridymite in Stannern, and it is briefly mentioned in Zbik and Gostin (1996b) but this is unsubstantiated by other authors.

Merrillite: Merrillite, a phosphate-bearing phase, contains minor Fe and Mg (3-4%), but shows REEs in very large abundances (5000-25000 more than C1 chondrites). They are LREE-enriched, have a pronounced negative Eu anomaly, and excluding Eu show a smooth decrease from La to Lu (Hsu and Crozaz, 1996). Crozaz (1979) also mentioned the presence of another phosphate, flourapatite, with U concentrations >20 ppm.

Zircon: Zircons occur as inclusions (the authors do not state which phase they are included in) in close association with ilmenite and chromite, but are at most 20 μm in size (Ireland and Bukovanska, 1992). A trace element and REE study of eighteen zircons showed similar Zr/Hf ratios (0.63) to lunar rocks (0.30-0.60), a noticeable negative Eu anomaly, U concentrations in the 30-80 ppm range, LREE values ranging from nearly chondritic to 100x chondritic, and fractionated HREE distributions corresponding to overall LREE abundances (Ireland and Bukovanska, 1992).

Whole Rock Composition:

The major element composition of Stannern has been compiled by numerous workers including Urey and Craig (1953), Engelhardt (1963), Duke and Silver (1967), McCarthy et al (1973), Kitts and Lodders (1998), Barrat et al (2000), and Barrat et al (2007). Many of these are surveys of previously available literature, including original analyses from 19th century researchers. These results are summarized in **Table 2**.

Minor and trace element chemistry are summarized in **Table 3**. Stannern (and other Stannern-trend eucrites) are enriched in incompatible trace elements and Ti, and show significant negative Eu, Sr, and Be anomalies standardized to chondritic values. Part of this trend is the decoupling of variations in Mg# with the concentrations of these incompatible elements; the Stannern trend is rather limited in its range of FeO/MgO but shows much higher range of incompatible element enrichment. The implication is that Stannern crystallized from a primary melt, as opposed to Nuevo Laredo-trend and main-group eucrites whose chemistry suggest a fractional crystallization model (or a significantly higher degree of partial melting) (see **Figure 12** for an example of the two trends from recent literature). Numerous authors

have attempted to reconcile these end-member models, but these are mostly beyond the scope of this paper; see Barrat et al (2007) for a recent summary of available literature.

Figure 13 shows REE data found in **Table 3**, normalized to chondritic values.

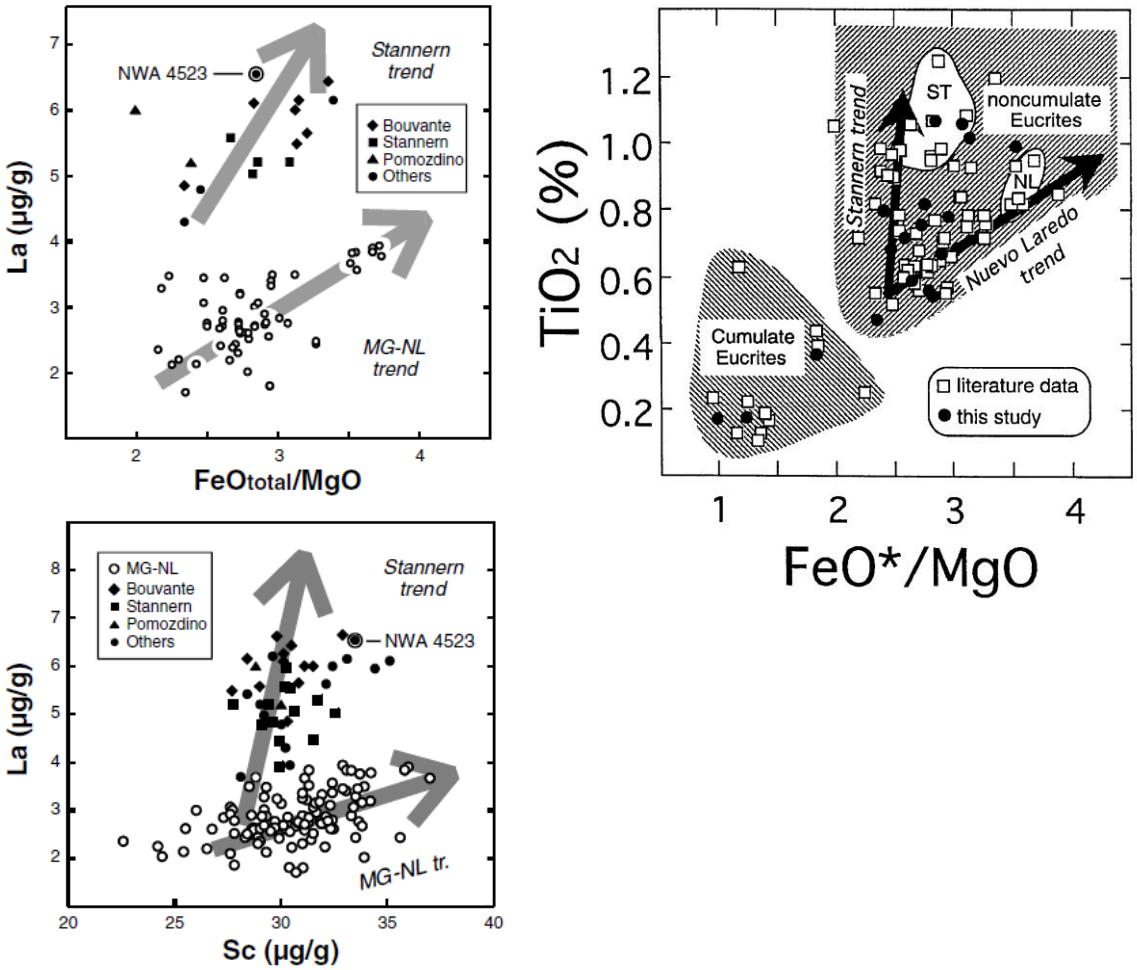

***Figure 12**: Figures from Barrat et al (2007) (left) and Barrat et al (2000) (above), illustrating the Stannern chemical trend. The circled white area marked "ST" represents measurements directly from the Stannern eucrite.*

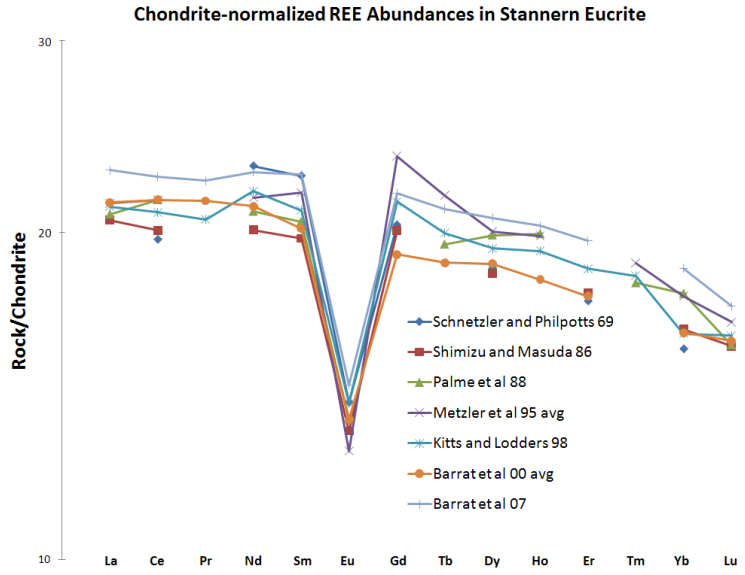

***Figure 13**: Chondrite-normalized abundances for REEs in Stannern, using data found in Table 3. Chondrite REE values are from Evensen (1978).*

Table 2: Major element composition data for the Stannern eucrite.

reference	*in* Urey and Craig (1953)	*in* Engelhardt (1963)		McCarthy et al (1973)	Kitts and Lodders (1998)	Barrat et al (2000)		Barrat et al (2007)
	Merrill (1925)	Lacroix(1925)	Silver and Maynes (1962)			ST1	ST2	
weight	--	--	--	--	--	--	--	1.0 g
SiO_2	47.94	49.12	49.33	49.7	49.2	--	--	--
TiO_2	0.41	0.58	0.96	0.98	0.98	1.07	1.06	1.08
Al_2O_3	11.19	13.39	12.34	12.33	12.2	12.05	13.14	12.75
FeO	20.05	17.16	17.92	17.78	18.1	19.58	19.7	18.58
MnO	--	0.21	0.5	0.525	0.51	0.54	0.55	0.55
MgO	7.14	6.8	6.36	6.97	7	6.86	6.4	6.98
CaO	10.36	10.72	10.58	10.67	10.6	10.39	10.5	10.99
Na_2O	0.75	0.4	0.6	0.62	0.54	0.58	0.58	0.56
K_2O	0.13	0.17	0.08	--	0.08	--	--	0.09
Cr_2O_3	0.35	0.31	0.29	0.34	0.3	0.33	0.29	0.33
P_2O_5	0.14	0.17	0.13	0.102	0.13	--	--	0.1
S%	0.31	--	--	--	0.19	--	--	--
H_2O^+	0.3	0.14	0.24	--	--	--	--	--
H_2O^-	--	0.3	0.02	--	--	--	--	--
Fe (met)	0.55	--	0.02	--	--	--	--	--
FeS	0.86	0.27	0.72	--	--	--	--	--
sum	**99.87**	**--**	**--**	--	**99.8**	--	--	--
technique :				X-Ray Flourescence Spec.		ICP-AES/ICP-MS		ICP-AES/ICP-MS

Table 3: Minor and Trace Element Chemistry for the Stannern Eucrite.

reference	**Heymann et al 68**	**Palme and Rammensee 81**		**Shimizu and Masuda 86**	**Palme et al 88**	**Paul and Lipschutz 90**
weight		287mg	265mg		.1006 g	
Ca ppm						
Na ppm	3780±80				4270 (b)	
K ppm					700 (b)	
P ppm						
Sc ppm	32±2	31.7 (b)	30.4 (b)		30.6 (b)	
Ti ppm						
V ppm						
Cr ppm	1780±100	2280 (b)	2030 (b)		2200 (b)	
Mn ppm	3970±120				4210 (b)	
Co ppm	4±2	3.8 (b)	3.7 (b)		7.18 (b)	6.13 (b)
Ni ppm					<10 (b)	
Cu ppm		9.6 (b)	0.8 (b)			
Zn ppm						7.72 (b)
Ga ppm					2.17 (b)	1.4 (b)
Ge ppm						
As ppb		7.3 (b)	35 (b)			
Se ppm	**Tera et al 70**				<0.7 (b)	0.405 (b)
Rb ppm	*0.696 (a)*					0.52 (b)
Sr ppm	*87.7(a)*			83.1 (a)	94 (b)	
Y ppm						
Zr ppm					89 (b)	
Nb ppm						
Mo ppb						
Ru ppm						
Rh ppm						
Pd ppb						
Ag ppb						71.9 (b)
Cd ppb						7.4±0.4 (b)
In ppb						0.17±0.04 (b)
Sn ppb						28 (b)
Sb ppb		105 (b)	3 (b)			
Te ppb						7.0±1.6 (b)
Cs ppb	**Schnetzler and Philpotts 69**					16.5 (b)
Ba ppm	*57.8 (a)*			45.3 (a)	53 (b)	
La ppm		5.31 (b)	5.12 (b)	5.02 (a)	5.08 (b)	
Ce ppm	*12.6 (a)*			12.85 (a)	13.7 (b)	
Pr ppm						**Blichert-Toft et al 02**
Nd ppm	*10.9 (a)*			9.52 (a)	9.9 (b)	*10.09 (d)*
Sm ppm	*3.47 (a)*	3.33 (b)	3.23 (b)	3.04 (a)	3.15 (b)	*3.189 (d)*
Eu ppm	*0.81 (a)*	0.82 (b)	0.79 (b)	0.762 (a)	0.782 (b)	
Gd ppm	*4.15 (a)*			4.1 (a)		
Tb ppm		0.79 (b)	0.81 (b)		0.73 (b)	
Dy ppm	*4.71 (a)*			4.66 (a)	5.05 (b)	
Ho ppm					1.13 (b)	
Er ppm	*2.87 (a)*			2.92 (a)		
Tm ppm					0.46 (b)	
Yb ppm	*2.58 (a)*	2.92 (b)	3.07 (b)	2.69 (a)	2.9 (b)	**Blichert-Toft et al 02**
Lu ppm	**Kleine et al 05**	0.42 (b)	0.45 (b)	0.399 (a)	0.4 (b)	*0.4147 (d)*
Hf ppb	*525 (d)*	2430 (b)	2440 (b)		2340 (b)	*2330 (d)*
Ta ppb		370 (b)	301 (b)		500 (b)	
W ppb	*48.3 (d)*	151 (b)	100 (b)			
Re ppb						
Os ppb						
Ir ppb					<3 (b)	
Pt ppb						**Paul and Lipschutz 90**
Au ppb		1.4 (b)	0.6 (b)		<1 (b)	10.8 (b)
Th ppb	**Stirling et al 05**	530 (b)	530 (b)	**Kuroda et al 66**	600 (b)	
U ppb	*153.05 ± 0.13 (d)*			*176±16 (b)*	160 (b)	210 (b)
	Tera et al 70					
Li ppm	*12.7 (a)*					
Be ppm				**Zhai and Shaw 94**		
B ppm				*0.92 (e)*		
S ppm					2790	
F ppm						
Cl ppm						
Br ppm				**Kuroda et al 66**		
I ppb				*635±20 (b)*		
Pb ppm						
Hg ppb						
Tl (ppb)						3.7±0.1 (b)
Bi (ppb)						2.63±0.08 (b)

technique: (a) Stable isotope dilution/MS; (b) INAA; (c) SEM/INAA; (d) ICP-MS, (e) PGNAA

Table 3: Minor and Trace Element Chemistry for the Stannern Eucrite.

reference	Metzler et al 95		Kitts and Lodders 98	Barrat et al 00		Mittlefehldt and Lindstrom 03	Barrat et al 07
weight	33.2 mg basalt clast	23.9 mg recryst. Matrix				583.8 mg weighted average of six samples	1.0 g
Ca ppm							
Na ppm	4560 (c)	3920 (c)	4031				
K ppm	770 (c)	643 (c)	646			543.45 (b)	
P ppm			556				
Sc ppm	29.8 (c)	31.9 (c)	31.2	29.4 (d)	27.7 (d)	30.13 (b)	30.2 (d)
Ti ppm			5860				
V ppm	62.3 (c)	61.4 (c)	77				56.9 (d)
Cr ppm	2210 (c)	2240 (c)	2081				
Mn ppm	3730 (c)	4150 (c)	3921				
Co ppm	10 (c)	9.1 (c)	6.6	7.5 (d)	8.4 (d)	5.16 (b)	3.83 (d)
Ni ppm	<12 (c)	<20 (c)	7	3 (d)	3 (d)		1.1 (d)
Cu ppm			9.5	10.4 (d)	9 (d)		5.07 (d)
Zn ppm	<25 (c)	<25 (c)	3.64	7.8 (d)	17.7 (d)		2.8 (d)
Ga ppm	<2.20 (c)	1.9 (c)	1.63	1.73 (d)	1.89 (d)		1.51 (d)
Ge ppm			0.08				
As ppb			20			365.33 (b)	
Se ppm	<0.50 (c)	<0.60 (c)	0.35			679.19 (b)	
Rb ppm			0.72	0.69 (d)	0.58 (d)		0.58 (d)
Sr ppm	<150 (c)	<80 (c)	88.8	89 (d)	92 (d)	95.79 (b)	92.7 (d)
Y ppm			27	29.85 (d)	27.12 (d)		32.13 (d)
Zr ppm	<80 (c)	<150 (c)	88	91.23 (d)	90.88 (d)	89.76 (b)	101 (d)
Nb ppm			5.5	6.68 (d)	6.69 (d)		8.2 (d)
Mo ppb			39				
Ru ppm							
Rh ppm							
Pd ppb							
Ag ppb			56				
Cd ppb			16.4				
In ppb			0.5				
Sn ppb							
Sb ppb			15.5			32.60 (b)	
Te ppb			7				
Cs ppb			15.6	16 (d)	16 (d)		16 (d)
Ba ppm	54 (c)	52 (c)	50.1	59.1 (d)	50.1 (d)	50.52 (b)	52.65 (d)
La ppm	5.22 (c)	5.18 (c)	5.166	5.21 (d)	5.21 (d)	4.74 (b)	5.58 (d)
Ce ppm	13.9 (c)	13.5 (c)	13.344	13.76 (d)	13.64 (d)	12.68 (b)	14.4 (d)
Pr ppm			1.98	2.07 (d)	2.05 (d)		2.15 (d)
Nd ppm	10.3 (c)	10.1 (c)	10.337	10.07 (d)	9.95 (d)	8.96 (b)	10.76 (d)
Sm ppm	3.34 (c)	3.36 (c)	3.227	3.16 (d)	3.05 (d)	2.96 (b)	3.48 (d)
Eu ppm	0.78 (c)	0.68 (c)	0.808	0.779 (d)	0.782 (d)	0.75 (b)	0.84 (d)
Gd ppm	4.7 (c)	4.9 (c)	4.357	4.01 (d)	3.79 (d)		4.44 (d)
Tb ppm	0.79 (c)	0.83 (c)	0.748	0.724 (d)	0.681 (d)	0.69 (b)	0.787 (d)
Dy ppm	5.12 (c)	5.06 (c)	4.91	4.95 (d)	4.56 (d)		5.24 (d)
Ho ppm	1.14 (c)	1.11 (c)	1.09	1.06 (d)	0.992 (d)		1.15 (d)
Er ppm			3.073	3 (d)	2.8 (d)		3.26 (d)
Tm ppm	0.45 (c)	0.51 (c)	0.467				
Yb ppm	2.91 (c)	2.86 (c)	2.663	2.81 (d)	2.53 (d)	2.58 (b)	3.06 (d)
Lu ppm	0.42 (c)	0.42 (c)	0.408	0.421 (d)	0.386 (d)	0.39 (b)	0.434 (d)
Hf ppb	2340 (c)	2410 (c)	2360	2350 (d)	2220 (d)	2174.54 (b)	2510 (d)
Ta ppb	340 (c)	340 (c)	405	368 (d)	348 (d)	295.88 (b)	441 (d)
W ppb	<100 (c)	<150 (c)	126	220 (d)	132 (d)		174 (d)
Re ppb							
Os ppb							
Ir ppb	<2 (c)	<2 (c)	0.12				
Pt ppb							
Au ppb	<1 (c)	<3 (c)	6.85			20.81 (b)	
Th ppb	600 (c)	590 (c)	610	680 (d)	564 (d)	550.50 (b)	700 (d)
U ppb	160 (c)	147 (c)	187	172 (d)	163 (d)	285 (b)	177 (d)
Li ppm			10				12.39 (d)
Be ppm							0.44 (d)
B ppm			0.339				
F ppm			48				
Cl ppm			34.5				
Br ppm			0.06			0.100 (b)	
I ppb			830				
Pb ppm			0.119				1.59 (d)
Hg ppb			9120				
Tl (ppb)			2.14				
Bi (ppb)			4.5				

technique: (a) Stable isotope dilution/MS; (b) INAA; (c) SEM/INAA; (d) ICP-MS, (e) PGNAA

Radiogenic Isotopes: Early K-Ar work on Stannern resulted in a range of ages from 2.95 Ga (Vinogradov et al, 1960) to 3.79 Ga (Kirsten et al, 1963), coincident with an early U,Th-^{4}He age of 3.6 Ga (Hintenberger et al, 1962). Megrue (1966) determined a K-Ar age of 3.98 ± 0.12 Ga, interpreting this date to represent late gas retention in slow-cooling objects that began crystallization sometime around 4.6 Ga (as determined by Rb-Sr ages in other similar achondrites by Gast, 1962; and Pinson et al., 1965). This conclusion was challenged by Burnett and Wasserburg (1967), who argued for further comparison to Rb-Sr and Pb-U-Th ages from different components to determine whether or not the age from Megrue (1966) actually represented a distinct event. Ar-Ar age dating from Podosek and Huneke (1973) was also inconclusive (**Figure 14**); it indicated gas retention ages spanning 3.5-3.9 Ga, which the authors suggested as evidence of an atypical disturbance, perhaps indicative of inherited ^{40}Ar mixing with normal diffusive Ar loss. Heymann et al (1968) also obtained U,Th-^{4}He and K-Ar ages around these values (3.9 Ga and 3.8 Ga, respectively).

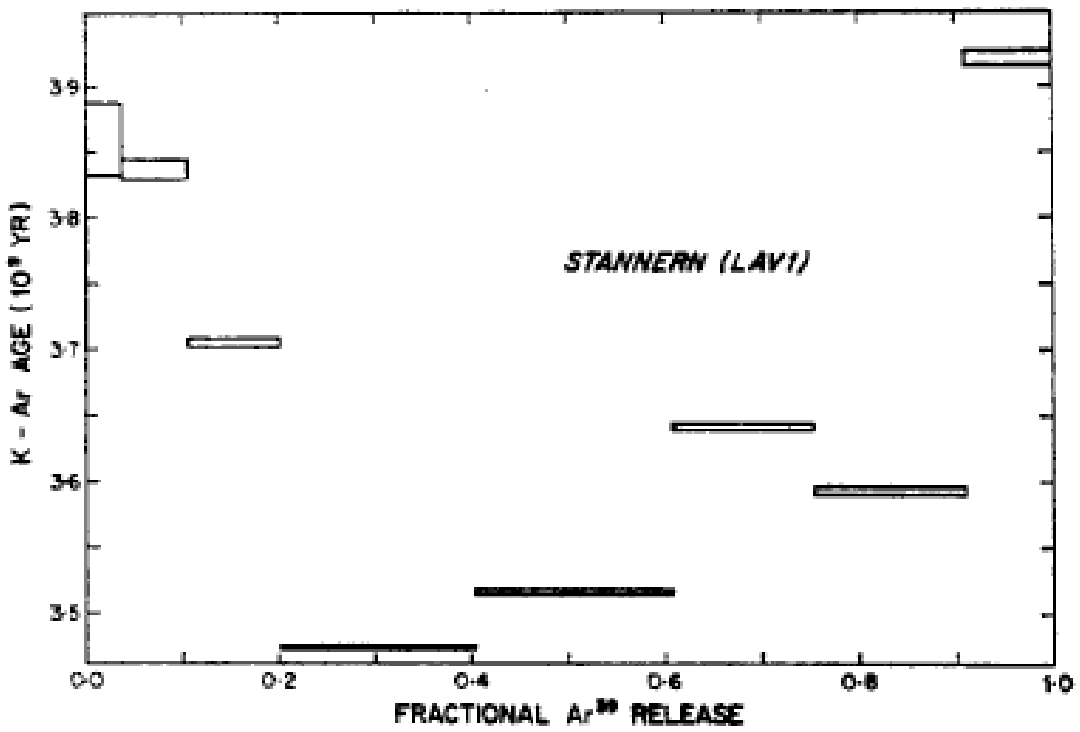

***Figure 14**: Pattern of apparent K-Ar ages in release fractions of Stannern. Podosek and Huneke (1973), Figure 2.*

Lugmair and Scheinen (1975), using Sm-Nd, proposed an initial crystallization age around 4.48 ± 0.07 Ga (**Figure 15**); because of the scatter in their data, they suggested that the parent material differentiated and solidified earlier (citing a Juvinas crystallization age 4.56 Ga from Lugmair, 1974) but was altered by a later violent metamorphic event at 3.7 Ga or later. This event would have been responsible for the slight disturbances in the Sm-Nd data, but would have had a much greater impact on U,Th-^{4}He, U-Th-Pb, Ar-Ar, K-Ar, and Rb-Sr ages, including the Sr-isotopic ages from Papanastassiou and Wasserburg (1969) (4.36 ± 0.26 Ga) and Papanastassiou (1970) (4.1±0.7 Ga). Birck and Allegre (1978) came to a similar conclusion; using Rb-Sr ages from mineral separates (deriving an overall age of 3.3 ± 0.5 Ga – see **Figure 16**), and noting that different separates from Stannern were not in equilibrium, they proposed an initial crystallization age around 4.55 Ga followed by later metamorphism at 3.3 Ga.

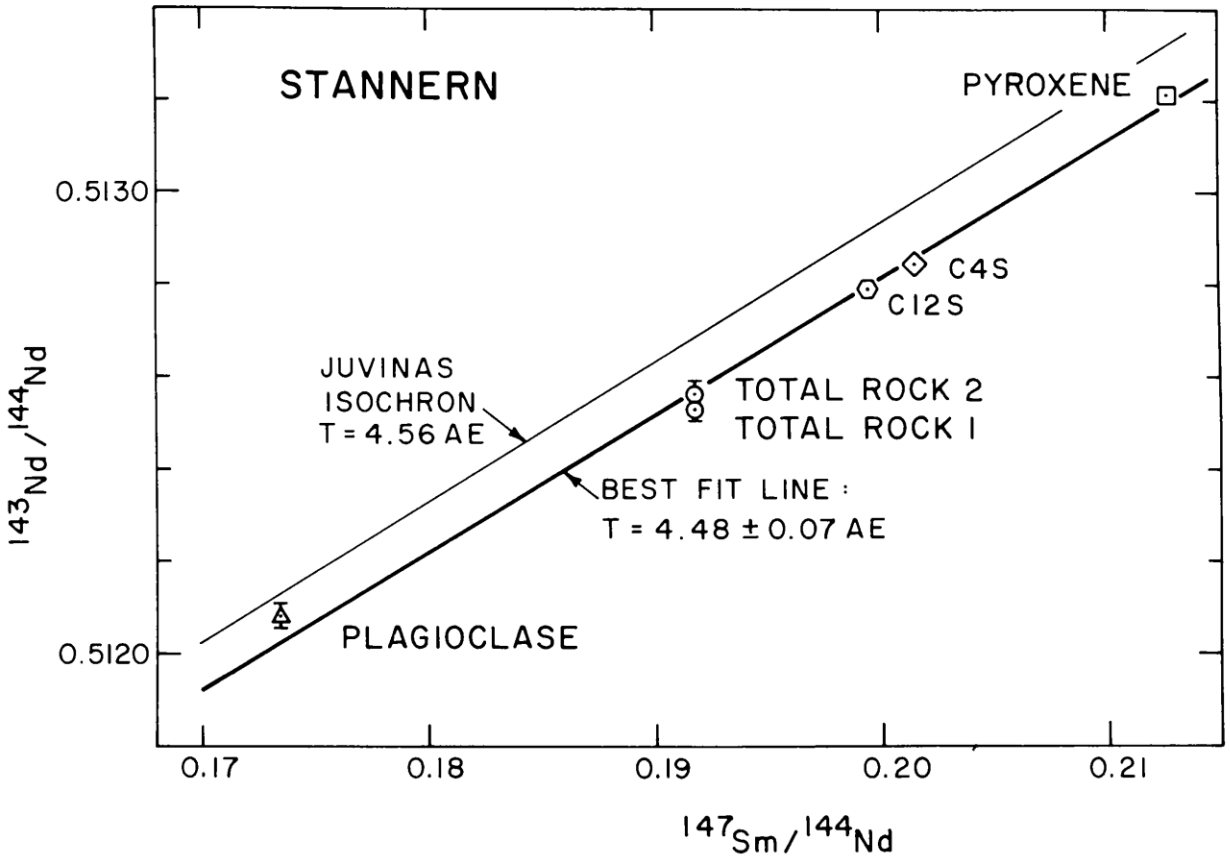

***Figure 15**: Sm-Nd evolution diagram for Stannern (including an isochron previously measured for Juvinas); though there is some scatter in the data, a best fit line can be drawn at 4.48 ± 0.07 Ga. Lugmair and Scheinin (1975), Figure 1.*

Ireland and Bukovanska (1992) analyzed Stannern zircons and determined a ^{207}Pb-^{206}Pb age of 4.550 ± 0.010 Ga, which is in agreement with the Sm-Nd age from Lugmair and Scheinen (1975), a more recently measured Sm-Nd age of 4.46 ± 0.08 Ga from Blichert-Toft et al (2002), and a whole eucrite Lu-Hf age of 4.550 Ga (Patchett and Tatsumoto, 1980). This suggests that the zircons were not affected by the events that disturbed other radiometric isotopic systems (especially Rb-Sr). However, other discrepant Pb-Pb ages from pyroxene and plagioclase separates (e.g., 4.128 ± 0.016 Ga from Tera et al, 1997) add further evidence for later disturbances after initial crystallization.

Hf-W systematics for Stannern were investigated by Kleine et al (2005). Both metal and non-metal fractions of the meteorite were examined, and a ^{180}Hf/^{184}W age of 4.564 ± 0.002 Ga was obtained (**Figure 17**); however, based on different isotopic ratios of W between Stannern metal and the eucrite whole rock value, Kleine et al (2005) contended that the Hf-W system in Stannern was re-equilibrated 0.5-3.6 million years after crystallization, and thus the Hf-W age represents thermal metamorphism very shortly after initial crystallization. This could be accomplished by slow cooling in the deep interior of Vesta.

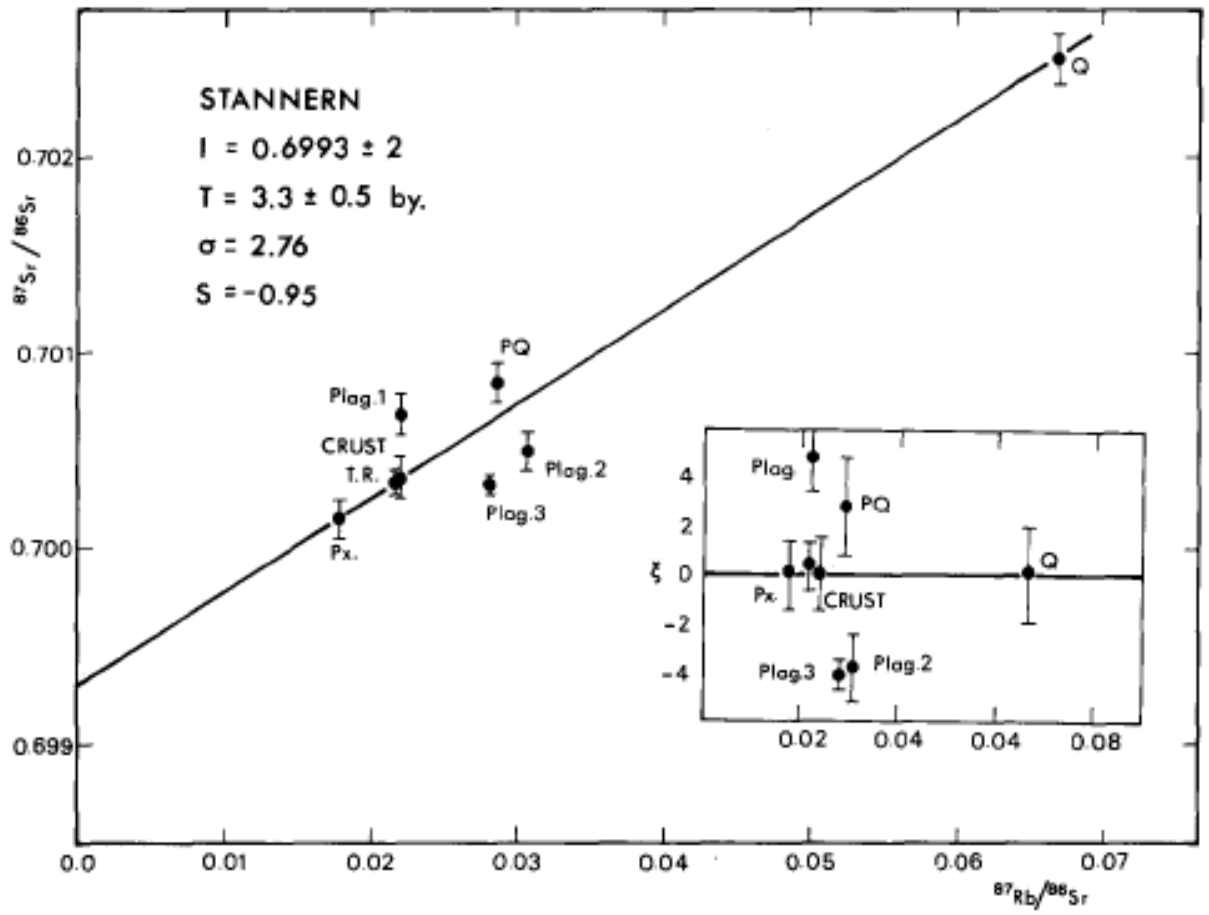

***Figure 16**: Rb-Sr evolution diagram for Stannern minerals. Birck and Allegre (1978), Figure 5.*

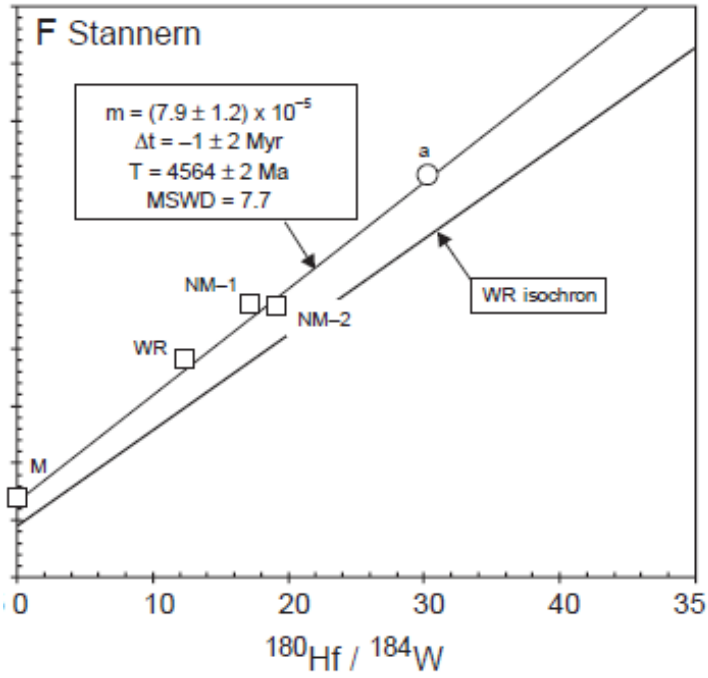

***Figure 17**: Hf-W systematics in Stannern. Kleine et al (2005), taken from Figure 1.*

Pu-Xe ages have also been very useful for comparison; Michel and Eugster (1994), Shukolyukov and Begemann (1996b), and Miura et al (1998) determined fission-derived Xe retention times of 4.442 Ga, 4.460 Ga, and 4.434 Ga respectively, well within the error established by Lugmair and Scheinen (1975) for their Sm-Nd ages. However, the fact that these ages do not correlate as well with zircon Pb-Pb ages (Ireland and Bukovanska, 1992) and the post-crystallization Hf-W age from Kleine et al (2005) suggests that this system was disturbed to some

degree by the same event affecting other isotopes, including Sm-Nd.

The timing of the event responsible for the widely-observed isotopic disturbances was clarified by the work of Kunz et al (1992) and Kunz et al (1995), who cited low temperature and high temperature closing ages for the K-Ar system in Stannern (3.3 ± 0.2 Ga and 4.0 ± 0.2 Ga), as well as an age for the last degassing event (3.5 ± 0.1 Ga). Bogard and Garrison, 1992, also cite a degassing event clustered around 3.8-4.1 Ga, which may be related to the similarly-timed lunar cataclysm. Bogard, 1995, summarizes a number of previously obtained isotopic ages from different systems and puts them in the context of those obtained from other HED meteorites.

Analysis of Mn-Cr in Stannern was undertaken by Trinquier et al (2008), who measured a $^{55}Mn/^{52}Cr$ ratio of 2.16 and an $\varepsilon^{53}Cr$ value of 0.63 ± 0.07. These values are sub-chondritic, as are those for Earth, which is consistent with volatile Mn fractionation relative to Cr (Trinquier et al, 2008).

^{129}I-^{129}Xe and ^{244}Pu-^{136}Xe formation intervals (Ξ_{129} and Ξ_{244}, representing the time between the cessation of solar (^{129}I) and galactic (^{244}Pu) nucleosynthesis and the formation of the meteorite) have been reported for Stannern by Kuroda et al (1966), with both Ξ_{129} and $\Xi_{244} \approx 300$ million years. This is mostly concordant with a U-^{136}Xe formation interval (Ξ_{136}) of 255 ± 40 Ma and an additional ^{129}I-^{129}Xe formation interval (Ξ_{129}) of 275 ± 50 Ma from Rowe (1967).

Cosmogenic Isotopes and Exposure Ages:

A summary of researchers and their cosmogenic noble gas exposure ages can be found in **Table 4**, below. Each source contains further information on the actual isotopic compositions of the noble gases. Large anomalies in cosmogenic xenon isotopes (i.e., light xenon) in Stannern were reported by Rowe et al (1965), Marti et al (1966), and Rowe (1967), the latter of which summarizes much of the early Xe isotope work in achondrites.

Table 4: Noble-gas exposure ages for Stannern. All ages are in millions of years.

	Megrue (1966)	Eugster et al (1967)	Heymann et al (1968)	Schultz and Freundel (1986)	Freundel et al (1986)
Ages					
^{3}He	32.5±1.5		37		
^{21}Ne	22.2±1				
^{38}Ar					38.6±1.8
^{78}Kr					
^{81}Kr		41.9±1.6		41.1±1.3, 42.0±2.1, 41.8±1.9	
^{126}Xe					

	Eugster and Michel (1995)	Shukolyukov and Begemann (1996b)	Miura et al (1998)	Takeda et al (2007)
Ages				
^{3}He	21.9±3.0		22.7	21.5
^{21}Ne	28.6±4.5		32.7	27.1
^{38}Ar	47.8±12.0		38.7, 42.2	44.4
^{78}Kr	40.3±8.0			
^{81}Kr	41.9±1.6		35.1±0.7	
^{126}Xe	37.5±7.0	40.4 ± 0.8 my		

Other Isotopes: Taylor et al (1965) measure oxygen isotopes in a variety of meteorites, and found that the $\delta^{18}O$ values for Stannern (4.4‰ for plagioclase, 4.1‰ for pyroxene, and 4.3‰ calculated for the whole rock) coincided with those for other basaltic achondrites, hypersthene achondrites, and mesosiderites, suggesting a common parent body. Oxygen isotopes were also measured in two Stannern fragments by Wiechert et al (2004), who found an average $\delta^{18}O$ of 3.697‰, an average $\delta^{17}O$ of 1.756‰, and values of $\Delta^{17}O$ at -0.210 ± 0.013 and -0.200 ± 0.022, falling well within the ranges that were measured for overall HEDs. Slightly higher values were obtained by Greenwood et al (2005), with $\delta^{18}O$ = 3.803‰ ± 0.068‰, $\delta^{17}O$ = 1.748‰ ± 0.026‰, and $\Delta^{17}O$ = -0.245 ± 0.009, but were still within the HED values measured in the same study.

Zhai et al (1996b) and Zhai and Shaw (1994) measured B isotopic ratios for Stannern, deriving an estimate of $\delta^{11}B$ at -6.90. This value is more negative than other measured eucrites, and more negative than lunar samples measured in the same study, but all eucrites were within literature values for the total earth range.

Weyer et al (2005) measured bulk $\delta^{56}Fe$ for Stannern; their measured value of 0.012 ± 0.020 falls well within their values for bulk silicate earth, and very similar to other eucrites, SNC meteorites, pallasite metals, and pallasite silicates. This in turn suggests that iron was well-mixed during early solar system processes (Weyer et al, 2005). Other iron isotopic measurements were undertaken by Schoenberg and von Blanckenburg (2006), who found $\delta^{56}Fe$ = -0.003 ± 46, $\delta^{57}Fe$= -0.017 ± 73, and $\delta^{58}Fe$= -0.05 ± 41, similar to other eucrite and inner solar system values.

^{10}Be (measured) and ^{26}Al (literature values) were summarized by Aylmer et al (1988), with ^{10}Be ranging from ~16-24 dpm/kg and ^{26}Al ranging from ~90-130 dpm/kg. These values are contradictory; as a large eucrite, Stannern would be expected to have low ^{10}Be values (because of shielding), but the corresponding ^{26}Al values are too high (Aylmer et al, 1988). However, they can be reconciled using a pre-atmospheric radius of 100 g/cm^2 (Aylmer et al, 1988), significantly lower than the previously reported value of 150-300 g/cm^2 (Freundel et al, 1986).

$^{40}Ca/^{44}Ca$ was reported by Shih et al (1993) as 47.139 ± 0.004.

Experiments: Hiroi et al (1995) and Hiroi and Pieters (1998) measured reflectance spectra for Stannern and other HED achondrites, exploring the link between the HED meteorites, Vestoids, and the Asteroid 4 Vesta; the first paper contains the initial results for Stannern and both contain discussions and conclusions from the data.

Some authors (e.g., McCarthy et al, 1973; Mittlefehldt, 1992) have used Stannern compositional data (both major and trace elements) to theoretically model the HED parent body composition; the use of Stannern and other Stannern-trend eucrites in this type of modeling, in conjunction with main group and Nuevo Laredo-trend eucrites, is essential to deriving a common parentage for these dichotomous chemical compositions.

Stolper (1977a) performed low-pressure (1 atm) melting and quenching experiments on numerous eucritic compositions (including Stannern) to experimentally determine basic phase relations and the crystallization sequence for HED meteorites. Stolper concluded that the eucrites were formed by a sequence of partial melts from a source region composed of olivine (~Fo_{65}), pyroxene (~Wo_5En_{65}), plagioclase (~An_{94}), Cr-rich spinel, and metal (~6-8% Ni, 0.5% Co). According to this model, the

composition of Stannern would be produced by a 5-10% partial melt of this source region; as Stannern chemistry is very near the peritectic point for the proposed source composition, the first partial melts would be expected to produce Stannern-like major element patterns. Consolmagno and Drake (1977) used theoretical modeling on a slightly different parent source composition (50% olivine, 30% metal, 10% orthopyroxene, 5% clinopyroxene, and 5% plagioclase), and determined that Stannern probably represents an erupted basalt from a low degree (4%) of partial melting.

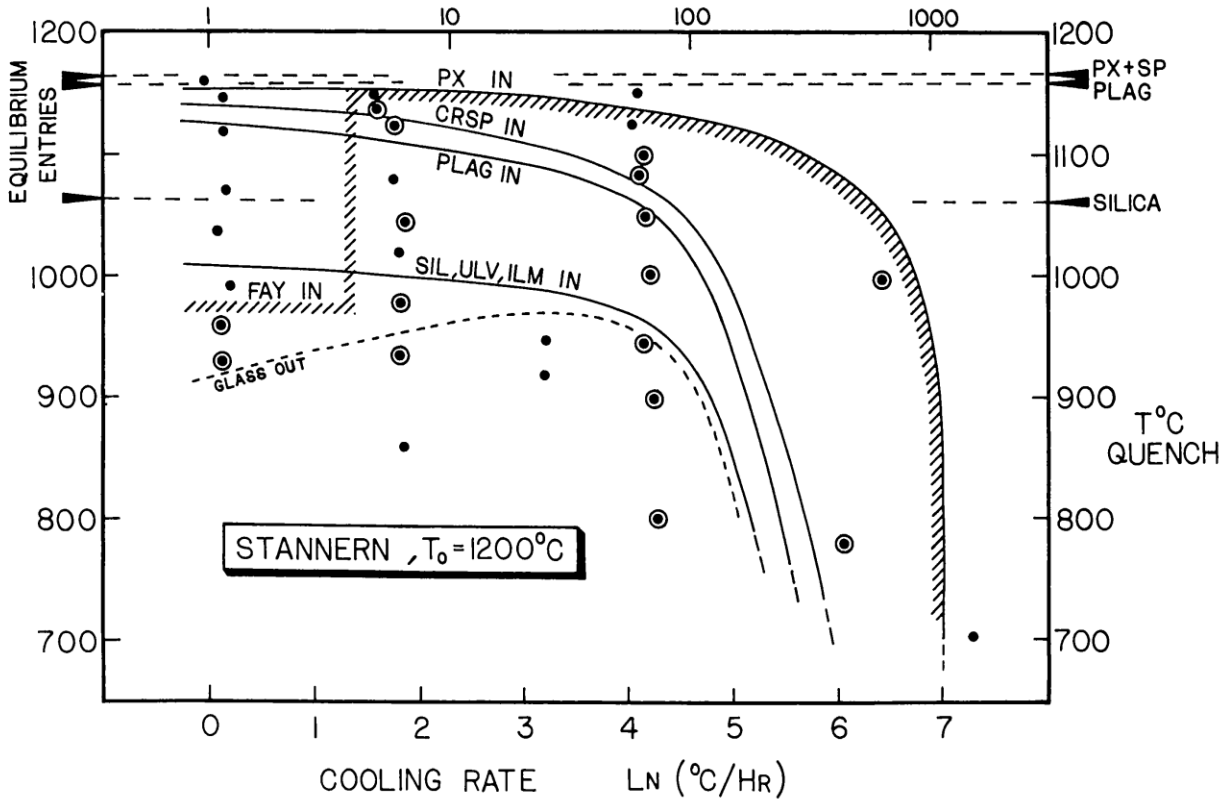

***Figure 18**: Phase appearance temperature as a function of cooling rate for Stannern samples that were initially melted to ~1200°C for 10 hours. Walker et al (1978), Figure 1.*

Walker et al (1978a) subjected ground samples of Stannern to different degrees of superheating and cooling rates; these experiments were undertaken to study the textural features in the meteorite and to attempt their reproduction in the lab. Walker et al (1978a) were able to produce a diagram (**Figure 18**) detailing the first appearance of mineral phases with cooling, and also reproduced a fasciculate, sheaf-like intergrowth texture seen variably in Stannern. They also concluded that the range of clasts seen in Stannern could be produced by cooling rates from 0.1 to 100°C/hr, or within three meters of the chill margin of a small magma body. Similar experiments were detailed by Powell et al (1980), indicating that Stannern probably produced zoned pyroxene crystals during magmatic cooling, but these were probably erased by extensive low temperature chemical re-equilibration. This equilibration (and later brecciation) also erased any evidence of immiscible liquids in the mesostasis, as well as the evidence for mesostasis itself, though immiscible liquids probably formed at the cooling rates determined by Walker et al (1978) for Stannern.

Metamorphism and Shock Effects: Numerous studies have discussed the relatively rapid initial igneous crystallization sequence that Stannern and other eucrites must have followed (e.g., Walker et al, 1978a).

It is clear, however, from numerous textural and chemical clues, that Stannern has been chemically re-equilibrated (Harlow and Klimentidis, 1980; Takeda et al, 1983; Brearley et al, 1993; Metzler et al, 1995; Yamaguchi et al, 1996). However, these same clues do not indicate recrystallization of most material in Stannern, and thus this re-equilibration must result from only a few possible causes: slow cooling and extensive re-equilibration between melt and mesostasis, shock effects, or some combination of shock effects and later heating (Phinney et al, 1993).

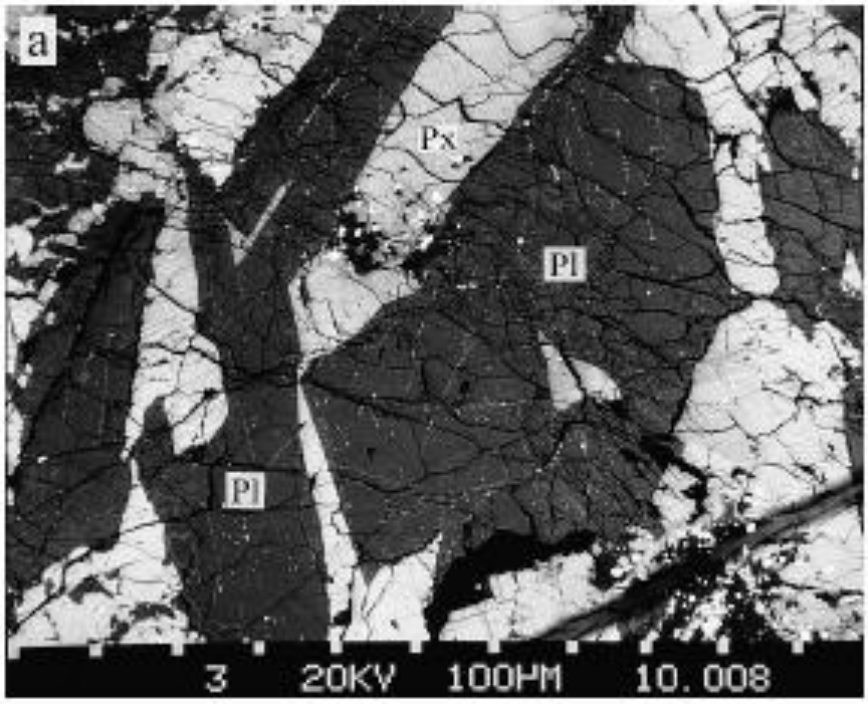

Figure 19*: Shocked plagioclase in Stannern, containing cleavages, cracks, and shock-induced fractures. The distance between the white bars at the bottom is 100 µm. Chen and El Goresy (2000), Figure 1.*

Specific metamorphic textures and chemistry include metamorphosed mesostasis (Takeda et al, 1983), considerable clouding, homogenization, and exsolution of pyroxenes (Harlow and Klimentidis, 1980; Takeda et al, 1983), lack of Fe/Mg zoning but preservation of calcium zoning in pyroxenes (Takeda et al, 1983; Yamaguchi et al, 1996; **Figure 8**), gradations from igneous to granular textures showing polygonal pyroxenes and plagioclase with curved boundaries (Yamaguchi et al, 1996), slightly recrystallized clastic matrix (Yamaguchi et al, 1996), and up to 2 mm-sized intrusive melt dikes with zoned pyroxene crystals (Metzler et al, 1995). Pyroxene homogenization in Stannern is classified as type 4 by the classification scheme of Takeda and Graham (1991).

Shock features in Stannern, besides the obvious macro-scale brecciation, are represented by anomalous plagioclase compositions (Miura and Kato, 1991), shock-induced cracks, cleavages, and fractures in plagioclase (Engelhardt, 1963; Chen and El Goresy, 2000) (**Figure 19**), K-enriched areas of plagioclase corresponding to injection of K into healed cracks (Hervig et al, 1986), clouding and deformation twinning in plagioclase (Boctor et al, 1987), bent plagioclase lamellae (Engelhardt, 1963), bent and flame-shaped deformation lamellae in troilite (Engelhardt, 1963), deflected ilmenite twin lamellae (Engelhardt, 1963), irregular fractures in pyroxene (Engelhardt, 1963), and mosaicism in pyroxene (Boctor et al, 1987). The minimum pressure required to produce the mosaic texture in pyroxene is 200 kilobars (Boctor et al, 1987).

Engelhardt (1963) noted that some shock features appear to have been initiated before the complete crystallization of the meteorite! First, irregular fractures in hypersthene do not necessarily continue into

adjacent pigeonite, even those that are rimming hypersthene cores, and therefore hypersthene must have been shocked before pigeonite nucleation; and second, as the last mineral to crystallize, quartz shows no evidence of mechanical deformation. (However, fractures in hypersthenes are filled with quartz, which is thought to have crystallized after pigeonite; also, other later-crystallizing phases, i.e., ilmenite and troilite, show evidence of mechanical deformation.)

Other authors have described the presence of up to 500 µm pseudo-tachylite veins that appear to have been created *in situ* by shock, after the original igneous and brecciation textures, as they crosscut both clastic and matrix materials (Duke and Silver, 1967; Bobe, 1992; Metzler et al, 1995). These veins consist of dark, devitrified glass, and contain fragments of the adjacent host rock – an example can be found in **Figure 20** here, and Figure 8 in Metzler et al (1995).

Metzler et al (1995) summarizes these observations and proposes the following processes for Stannern formation: (1) crystallization of the primary magma, (2) slow subsolidus cooling or reheating, (3) impact brecciation, and (4) thermal metamorphism.

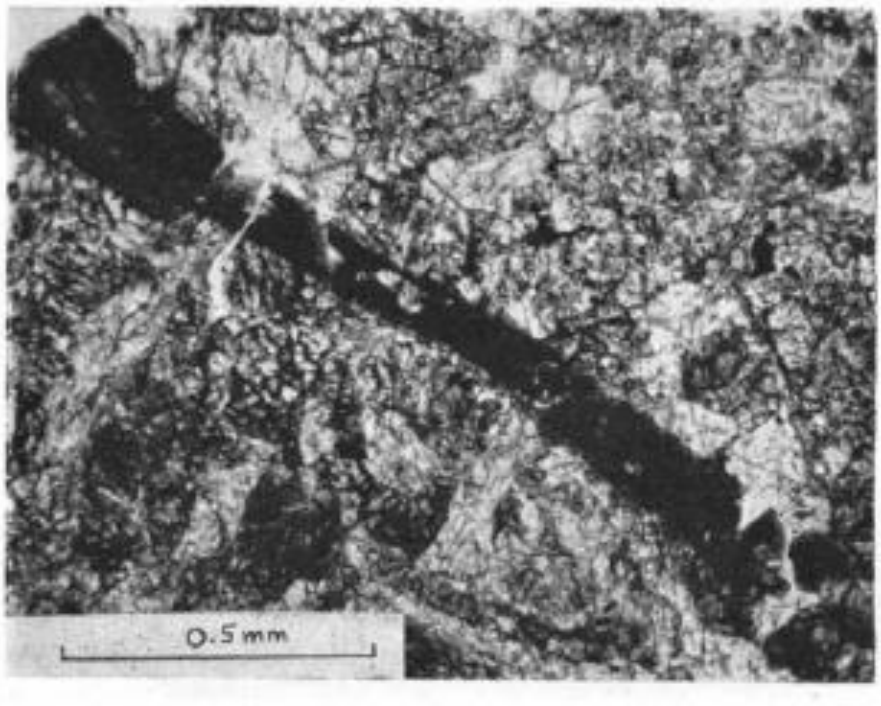

Figure 20*: Dark devitrified vein cross-cutting lithic fragments and matrix material. Plane light. Duke and Silver (1967), Figure 13.*

Constantinople: As an interesting side note, there was some historical question as to whether or not the Constantinople eucrite was a fragment of Stannern or if it was a separate fall – this question was addressed by Tschermak (1872), who determined that the major element composition and overall texture was very similar to Stannern. Heymann et al (1968), Table 5, contains a direct comparison of five major elements, cobalt, and noble gas data; a discussion in the text makes it evident that while there are many chemical similarities, there are enough anomalies to leave open the possibility that Constantinople was a separate fall.